The IDOL–UBE2D complex mediates sterol-dependent degradation of the LDL receptor

Li Zhang,[1,2,4] Louise Fairall,[3,4] Benjamin T. Goult,[3,4] Anna C. Calkin,[1,2] Cynthia Hong,[1,2] Christopher J. Millard,[3] Peter Tontonoz,[1,2,5] and John W.R. Schwabe[3]

[1]Howard Hughes Medical Institute, University of California at Los Angeles School of Medicine, Los Angeles, California 90095, USA; [2]Department of Pathology and Laboratory Medicine, David Geffen School of Medicine at University of California at Los Angeles, Los Angeles, California 90095, USA; [3]Henry Wellcome Laboratories of Structural Biology, Department of Biochemistry, University of Leicester, Leicester LE1 9HN, United Kingdom

We previously identified the E3 ubiquitin ligase IDOL as a sterol-dependent regulator of the LDL receptor (LDLR). The molecular pathway underlying IDOL action, however, remains to be determined. Here we report the identification and biochemical and structural characterization of an E2–E3 ubiquitin ligase complex for LDLR degradation. We identified the UBE2D family (UBE2D1–4) as E2 partners for IDOL that support both autoubiquitination and IDOL-dependent ubiquitination of the LDLR in a cell-free system. NMR chemical shift mapping and a 2.1 Å crystal structure of the IDOL RING domain–UBE2D1 complex revealed key interactions between the dimeric IDOL protein and the E2 enzyme. Analysis of the IDOL–UBE2D1 interface also defined the stereochemical basis for the selectivity of IDOL for UBE2Ds over other E2 ligases. Structure-based mutations that inhibit IDOL dimerization or IDOL–UBE2D interaction block IDOL-dependent LDLR ubiquitination and degradation. Furthermore, expression of a dominant-negative UBE2D enzyme inhibits the ability of IDOL to degrade the LDLR in cells. These results identify the IDOL–UBE2D complex as an important determinant of LDLR activity, and provide insight into molecular mechanisms underlying the regulation of cholesterol uptake.

[*Keywords*: LXR; cholesterol; nuclear receptor; ubiquitin ligase]

Supplemental material is available for this article.

Received April 1, 2011; revised version accepted May 16, 2011.

In eukaryotic cells, the degradation of many proteins is carried out by the ubiquitin system (Hershko and Ciechanover 1998). In this pathway, proteins are targeted for degradation through the covalent conjugation of the 76-amino-acid polypeptide ubiquitin. Conjugation proceeds via a three-step mechanism involving three enzymes (Dye and Schulman 2007). To initiate the process, a ubiquitin molecule is activated by the ubiquitin-activating enzyme E1 to form a high-energy intermediate with E1. The activated ubiquitin molecule is then transferred to a ubiquitin-conjugating enzyme, E2, to form an intermediate with the E2. Finally, association of this ubiquitin-charged E2 with an E3 ligase facilitates the conjugation of the ubiquitin molecule to the target protein. Specificity in ubiquitination pathways derives from the ability of individual E3 ligases to recognize a discrete set of target proteins (Pickart 2001).

There are two major categories of E3 ligases: HECT domain and RING domain E3 ligases. HECT domain E3 ligases mediate the conjugation of ubiquitin by formation of a HECT-ubiquitin intermediate, whereas RING domain E3 ligases facilitate the direct transfer of ubiquitin from the E2 to the substrate (Scheffner et al. 1993; Deshaies 1999). The ubiquitin system is organized into a hierarchical structure: A single E1 can transfer ubiquitin to several species of E2 enzymes, and each E2 acts in concert with either one or several E3 enzymes (Pickart 2001). Upon the completion of ubiquitin conjugation, the proteolysis of ubiquitinated proteins can be conducted in either the proteasome or the lysosome (Thrower et al. 2000). Ubiquitin-mediated protein degradation has been shown to play important roles in the control of numerous biological processes, including cell cycle progression (Koepp et al. 1999), signal transduction (Scheffner et al. 1990), and receptor down-regulation (Levkowitz et al. 1999).

The LDL receptor (LDLR) is a cell membrane protein essential for the uptake of LDL cholesterol and the regulation of plasma lipoprotein levels (Russell et al. 1984). Loss-of-function LDLR mutations in humans reduce hepatic LDL clearance, elevate plasma LDL levels, and accelerate atherosclerosis (Brown and Goldstein 1986). The abundance of the LDLR is regulated by both transcriptional

[4]These authors contributed equally to this work.
[5]Corresponding author.
E-mail ptontonoz@mednet.ucla.edu.
Article is online at http://www.genesdev.org/cgi/doi/10.1101/gad.2056211.

and post-transcriptional mechanisms in response to cellular cholesterol levels. The primary transcriptional regulator for LDLR is the SREBP-2 transcription factor (Hua et al. 1993). A reduction in the cholesterol levels in the endoplasmic reticulum (ER) triggers the processing of SREBPs to their mature nuclear forms and consequently activates the expression of genes important for the synthesis and uptake of cholesterol (Goldstein et al. 2006). Interestingly, activated SREBPs also induce the expression of Pcsk9, which binds LDLR and reduces its abundance on the plasma membrane (Maxwell and Breslow 2004; Park et al. 2004). Our laboratory recently identified a RING domain E3 ubiquitin ligase, IDOL, as an additional post-transcriptional regulator of the LDLR (Zelcer et al. 2009). Expression of the *IDOL* gene is induced by the sterol-activated transcription factors LXRα and LXRβ. Increased IDOL expression triggers the ubiquitination of the LDLR, leading to its internalization and degradation (Zelcer et al. 2009). Although it is postulated that IDOL acts directly on the LDLR, this has not been formally established. Since the expression of the *IDOL* gene is not regulated by SREBPs, the LXR–IDOL pathway represents an independent mechanism for feedback inhibition of the LDLR by cellular cholesterol levels.

The ubiquitination and subsequent degradation of the LDLR presumably depend on a cascade of ubiquitin transfer reactions carried out by E1, E2, and E3 enzymes. Although IDOL has been identified as the E3, the identity of the E2 involved has remained elusive. In the present study, we identify the ubiquitin-conjugating enzyme UBE2D family proteins (UBE2D1, UBE2D2, UBE2D3, and UBE2D4) as the E2 enzymes that collaborate with IDOL in LDLR ubiquitination. We also successfully obtained the crystal structure of the IDOL RING domain–UBE2D complex. Based on the information provided by the structure, we demonstrate that disruption of the interaction interface between IDOL and UBE2D prevents LDLR from being degraded by IDOL. Our results provide a better understanding of the molecular mechanism underlying the sterol-dependent regulation of LDLR protein levels.

Results

Identification of the E2 for IDOL autoubiquitination

Because it was not known whether IDOL could directly ubiquitinate the LDLR, we established an in vitro IDOL autoubiquitination assay in order to identify IDOL-interacting E2 enzymes. We hypothesized that, similar to other E3 ligases, IDOL might use the same E2 partner for both autoubiquitination and target (LDLR) ubiquitination. Autoubiquitination is characteristic of RING-type E3 ligases (Yang et al. 2000), and can be evaluated in vitro by incubating the E3 with its cognate E2 and the other factors required for ubiquitination. To establish the autoubiquitination assay, we first immunoprecipitated IDOL from HEK293 cells stably expressing an IDOL protein tagged with 3xFlag and Strep on its N-terminal end (TAP-IDOL). The efficacy of TAP-IDOL at degrading the LDLR was confirmed in cotransfection assays (Supplemental Fig. S1A). According to the HUGO Gene Nomenclature Committee, 38 E2 genes have been documented in the human genome (Bruford et al. 2008). Recent systematic studies have defined a subgroup of these E2 enzymes that preferentially participates in ubiquitination mediated by RING-type E3 ligases (Markson et al. 2009; van Wijk et al. 2009). We therefore screened a representative panel of the 19 E2 proteins belonging to this category. We expressed His-tagged E2 proteins in *Escherichia coli* (Fig. 1A), and then combined the crude lysates with immunoprecipitated IDOL, recombinant human UBE1, recombinant HA-tagged ubiquitin, and the ATP-generating system (Supplemental Fig. S2). Polyubiquitinated IDOL was detected in the presence of the four closely related members of the UBE2D family (UBE2D1–4), but not in the presence of any other E2 protein screened (Fig. 1B). This reaction was dependent on IDOL E3 activity, because UBE2D proteins failed to ubiquitinate an IDOL mutant harboring a cysteine mutation in the RING domain (C387A) (Fig. 1C; Supplemental Fig. S1B). This point mutation disrupts the function of the RING domain and abolishes the ability of IDOL to degrade itself or the LDLR (Zelcer et al. 2009). Furthermore, the ubiquitination reaction specifically targeted IDOL, because UBE2D proteins failed to induce the polyubiquitination of a TAP-EGFP protein immunoprecipitated in parallel with IDOL (Fig. 1D).

We next addressed the relative efficacy of the individual members of the UBE2D family in supporting IDOL autoubiquitination. We expressed UBE2D1, UBE2D2, UBE2D3, and UBE2D4 proteins in the same batch of *E. coli* cells, and used the same amount of each protein in autoubiquitination assays. We found that individual members of the UBE2D family exhibited similar capacity for forming polyubiquitinated IDOL (Fig. 1E). Polyubiquitin chains are usually formed via linkage on Lys48, Lys11, or Lys63 residues of ubiquitin (Pickart 2001). We sought to determine whether the autoubiquitination of IDOL was dependent on the Lys48, Lys11, or Lys63 linkage. We therefore provided exclusively wild-type ubiquitin, K11R ubiquitin, K48R ubiquitin, or K63R ubiquitin in the IDOL autoubiquitination assays. Interestingly, none of the mutant ubiquitins inhibited the autoubiquitination of IDOL (Fig. 1F), suggesting that the IDOL autoubiquitination catalyzed by the UBE2D enzymes did not exclusively use either the Lys48, Lys63, or Lys11 linkage.

UBE2D family proteins are the E2 enzymes for LDLR ubiquitination

In order to test the ability of IDOL to ubiquitinate LDLR in a cell-free system and determine whether the UBE2D family proteins are the E2 enzymes for LDLR ubiquitination, we sought to reconstitute an in vitro system in which IDOL, together with UBE1 and UBE2D enzymes, could mediate the transfer of ubiquitin to the LDLR. To this end, we expressed an LDLR-GFP fusion or GFP control in HEK293 cells and prepared membrane fractions by permeabilizing the plasma membrane and removing cytosolic proteins (Song and DeBose-Boyd 2004). We then mixed the

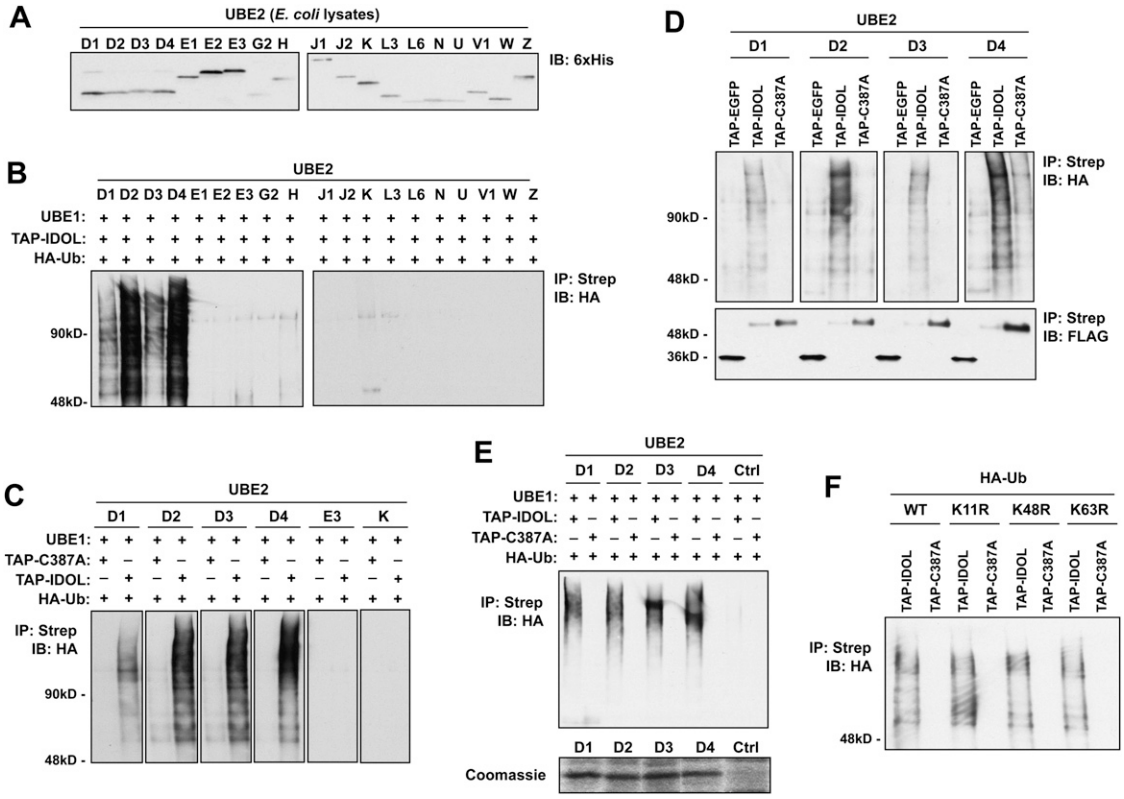

Figure 1. The UBE2Ds are specific partners for IDOL autoubiquitination. (*A*) Immunoblot of a panel of 19 human UBE2 enzymes that were expressed in *E. coli* as fusion proteins with 6xHis tags on their N termini. (*B*) Autoubiquitination of IDOL induced by UBE2D family proteins in an in vitro autoubiquitination assay. Immunoprecipitated TAP-IDOL was incubated with UBE1, HA-ubiquitin, and the indicated UBE2 proteins. IDOL ubiquitination was detected by immunoblotting for HA-tagged ubiquitin associated with IDOL. (*C*) Autoubiquitination of IDOL induced by UBE2D requires an active RING domain. Immunoprecipitated TAP-IDOL and TAP-IDOL C387A were incubated with UBE1, HA-ubiquitin, and the indicated UBE2 proteins. IDOL ubiquitination was detected by immunoblotting for HA-tagged ubiquitin associated with IDOL. (*D*) Autoubiquitination induced by UBE2D is specific to IDOL. Immunoprecipitated TAP-EGFP, TAP-IDOL, and TAP-IDOL C387A were incubated with UBE1, HA-ubiquitin, and UBE2D proteins. IDOL ubiquitination was detected by immunoblotting for HA-tagged ubiquitin associated with IDOL. The amounts of TAP-tagged proteins in the in vitro autoubiquitination assay were determined by immunoblotting using anti-Flag antibody. (*E*) UBE2D family proteins have similar capacity for inducing IDOL autoubiquitination. UBED1–4 protein levels used in the IDOL autoubiquitination assay were normalized by Coomassie staining of SDS-PAGE gels. Immunoprecipitated TAP-IDOL and TAP-IDOL C387A were incubated with UBE1, HA-ubiquitin, and the indicated UBE2D family proteins. IDOL ubiquitination was detected by immunoblotting for HA-tagged ubiquitin associated with IDOL. (*F*) IDOL autoubiquitination is not exclusively dependent on the Lys11, Lys48, or the Lys63 linkage of ubiquitin. Immunoprecipitated TAP-IDOL and TAP-IDOL C387A were incubated with UBE1, UBE2D2, and HA-tagged ubiquitin with the indicated lysine mutations. IDOL ubiquitination was detected by immunoblotting.

membrane preparation with recombinant UBE1, a crude lysate of *E. coli* expressing UBE2D2, tandem affinity-purified IDOL, recombinant HA-tagged ubiquitin, and the ATP-generating system (Supplemental Fig. S3). After the in vitro ubiquitination reaction, the membrane preparation was disrupted and the LDLR was immunoprecipitated. Ubiquitination was then assayed by immunoblotting. Remarkably, we found that polyubiquitinated LDLR was formed in the presence of UBE2D2 and IDOL, but not in the absence of UBE2D2 or the presence of RING domain mutant IDOL (C387A) (Fig. 2A).

In order to demonstrate that the UBE2D family proteins are the E2 enzymes that catalyze LDLR ubiquitination in vivo, we used a dominant-negative version of UBE2D2 lacking a critical cysteine residue within its catalytic domain (C85A) (Gonen et al. 1999). Expression of the dominant-negative UBE2D2 in HEK293 cells markedly inhibited IDOL-dependent LDLR degradation (Fig. 2B). In contrast, the expression of a dominant-negative mutant of an unrelated E2, UBE2H (C87A), did not inhibit LDLR degradation. Taken together, these results indicate that the UBE2D family proteins participate in the endogenous IDOL–LDLR ubiquitination cascade.

To provide further insight into the functional effects of IDOL and LDLR ubiquitination in cells, we treated cells expressing wild-type or RING MUT IDOL and LDLR with inhibitors of protein degradation. Consistent with prior work, transfection of RING MUT IDOL expression vector gave rise to markedly increased protein levels compared with wild-type IDOL expression vector, consistent with loss of autoubiquitination and degradation (Fig. 2C). Addition of the proteasomal inhibitor MG-132,

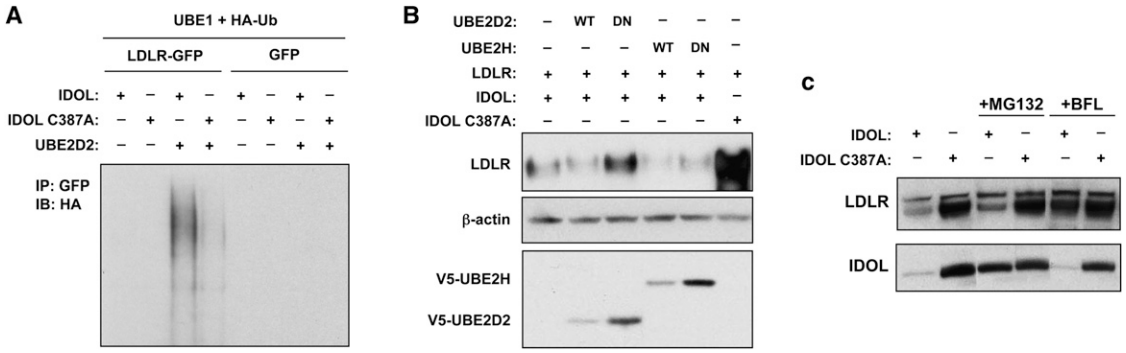

Figure 2. UBE2D family proteins are the E2 enzymes for LDLR ubiquitination. (*A*) Ubiquitination of the LDLR by UBE2D and IDOL in an in vitro ubiquitination assay. Membrane preparations of 293 cells expressing LDLR-GFP or GFP alone were incubated with UBE1, UBE2D2, tandem affinity–purified IDOL or IDOL C387A, and HA-ubiquitin. LDLR was then immunoprecipitated with an anti-GFP antibody. The ubiquitination of LDLR was detected by immunoblotting for HA-tagged ubiquitin associated with LDLR. (*B*) Expression of dominant-negative UBE2D2 inhibits the degradation of LDLR. Immunoblot analysis of protein levels in 293 cells transfected with wild-type (WT) or dominant-negative UBE2D or UBE2H, in addition to LDLR and IDOL. (*C*) Immunoblot analysis of IDOL and LDLR expression in response to inhibition of proteasomal or lysosomal degradation pathways. 293 cells were transfected for 24 h with expression vectors for wild-type or C387A mutant IDOL and LDLR. Cells were treated with MG-132 (25 μM) or bafilomycin (BFL; 100 nM), as indicated, 4 h prior to harvest.

but not the lysosomal inhibitor bafilomycin, stabilized wild-type IDOL protein levels, consistent with the hypothesis that ubiquitinated IDOL is degraded in the proteasome. In contrast, IDOL-dependent LDLR degradation was blocked by bafilomycin, but not by MG-132. These results strongly suggest that IDOL-dependent LDLR ubiquitination and IDOL autoubiquitination have distinct functional consequences and lead to distinct degradation pathways.

The IDOL RING domain interacts directly with UBE2D1

To further investigate IDOL–UBE2D interaction, we used NMR spectroscopy. The IDOL RING domain protein (residues 369–445) was expressed in *E. coli* and readily purified. The $^{1}H,^{15}N$ HSQC NMR spectrum indicated a stable and well-defined protein fold. However, the line widths suggested a molecular weight higher than would be expected for a 9-kDa protein. The interaction between the IDOL RING domain and UBE2D1 was studied by collecting $^{1}H,^{15}N$ HSQC spectra of a ^{15}N-labeled RING domain in the presence of increasing concentrations of unlabeled UBE2D1 (Fig. 3A). A number of resonances showed progressive changes in chemical shift indicative of a direct interaction. To further analyze this chemical shift data, we used a ^{13}C-^{15}N-labeled protein IDOL RING domain (residues 369–445) to complete the backbone assignment. The weighted $^{1}H,^{15}N$ chemical shifts in IDOL RING induced by UBE2D1 were plotted as a function of residue number (Fig. 3B), and this analysis showed that the interaction is specific and involves residues M388, V389, C390, C391, and C411 of the IDOL RING domain, with chemical shift perturbations >0.05 ppm (δΔ ppm) (Fig. 3B). Thus, NMR analysis confirmed the direct interaction between IDOL and UBE2D1 suggested by our in vitro screen.

Structure of the IDOL RING–UBE2D1 complex

In addition to the NMR chemical shift titrations, we determined the crystal structure of the IDOL RING domain (residues 369–445) both alone (Fig. 3C,D) and in complex with UBE2D1 (Fig. 4A–E; Supplemental Fig. S4; Table 1). It was not immediately apparent from the protein sequence which residues of the IDOL RING domain would chelate zinc, due to the presence of multiple cysteine and histidine residues in addition to those normally observed in RING domains. However, the structure reveals that the IDOL RING domain uses seven cysteines and one histidine to coordinate two zinc ions in a conventional pattern (Barlow et al. 1994), with the protein structure interleaved around the zinc ions (Fig. 3C). An N-terminal helix precedes the IDOL RING domain. The whole structure forms a homodimer in the crystal lattice. This is mediated in part by the N-terminal helix, but mainly through a tight interface between the RING domains that have a highly complementary shape, such that the buried surface area of the dimerization interface is 1862 $Å^2$ (Fig. 4B). The IDOL RING dimerization interface is one of the most ordered parts of the IDOL–UBE2D1 complex structure (Supplemental Fig. S4A), with multiple nonpolar amino acids (Val431, Leu433, Ile395, and Pro434) at the interface (Fig. 4C). In addition to the hydrophobic interactions, there are backbone interactions between Tyr432 and Gly403′. Tyr432 is also involved in a stacking interaction with the histidine ring of His 404′ (Fig. 4C). The side chain of Gln429 makes a hydrogen bond with the backbone of Pro401′. Three leucine residues (Leu374, Leu378, and Leu381) in the helix preceding the zinc-binding domain also appear to contribute to dimerization, but this part of the structure is less well ordered (Supplemental Fig. S4A).

In the structure of the complex, the IDOL–UBE2D1 interface is well ordered and, like the dimerization

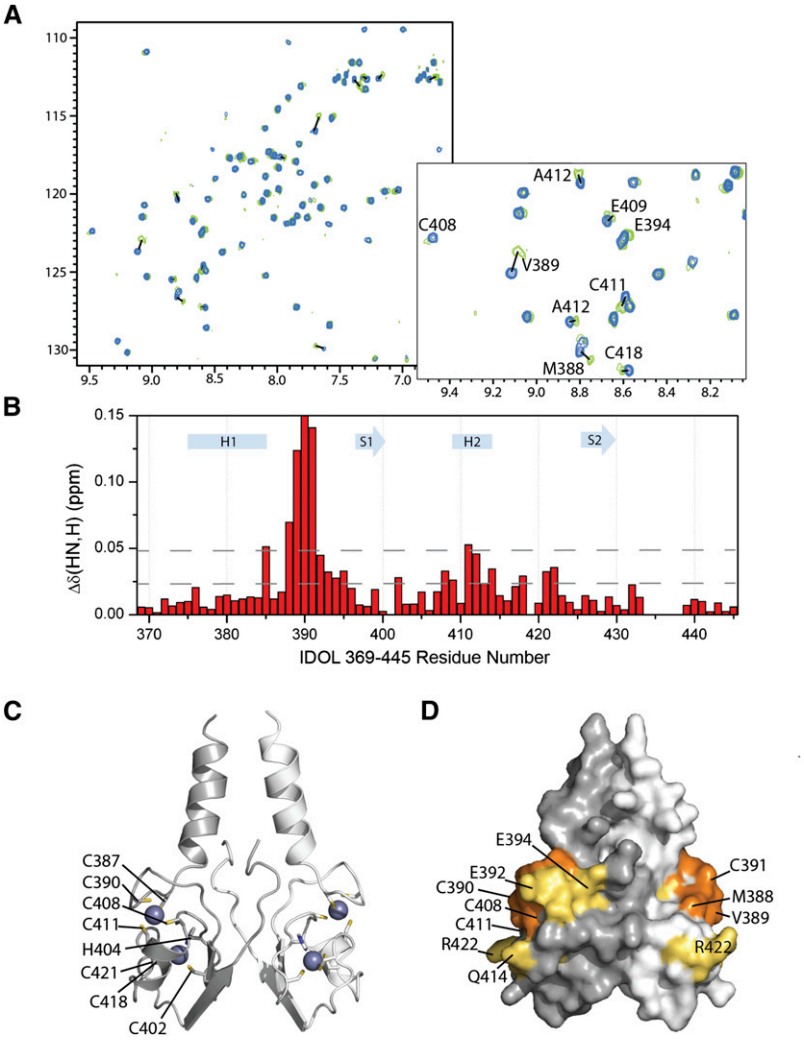

Figure 3. NMR chemical shift mapping of the IDOL RING domain with UBE2D1. (*A*) $^{1}H,^{15}N$ HSQC spectra of 150 μM ^{15}N-labeled IDOL RING domain in the absence (blue) and presence (green) of UBE2D1 at an equimolar ratio. (*B*) Weighted shift map obtained from the [$^{1}H,^{15}N$]-HSQC spectra of the IDOL RING domain with the addition of UBE2D1. (*C*) Ribbon representation of the crystal structure of the IDOL RING domain. (*D*) Surface representation of the IDOL RING domain, with the most significant shifts (>0.05 ppm) shown in orange and smaller perturbations (>0.025 ppm) shown in yellow.

interface, is predominantly hydrophobic (Fig. 4D,E). The core of the interface consists of amino acids Val389, Leu415, and Pro419 of IDOL packing on Phe62, Pro61, and Pro95 on UBE2D1. UBE2D1 side chains Lys4, Arg5, and Ser94 make hydrogen bonds to the side chain of Glu392 and the backbone of Met388 and Pro419 of IDOL, respectively. Arg422 of IDOL makes hydrogen bonds with the backbone of Gln92. The interface observed in the crystal structure is consistent with the NMR chemical shift mapping. Interestingly, the RING:RING dimer interface is somewhat rearranged in the complex with UBE2D1 so as to form a tighter interface compared with the RING dimer alone (Supplemental Fig. S4B). The two Pro434 residues within the RING dimer move 4.3 Å toward each other, tightening the homodimeric interface in the complex with UBE2D1 compared with the RING domain alone (Supplemental Fig. S4C). It is intriguing to speculate that there may be some cooperative rearrangement on binding the E2, but the influence of crystal packing cannot be ruled out.

The IDOL RING–UBE2D1 structure is similar to the structure of UBE2D2 in complex with the cIAP2 RING (Mace et al. 2008), and explains why IDOL can interact with all members of the UBE2D family of E2 enzymes. The two structures vary, however, in the orientation of the helix preceding the zinc-binding RING domain. The interface between the IDOL RING and UBE2D1 is not as extensive as the RING:RING dimer interface and buries only 1140 $Å^2$, which would suggest that the complex may be rather transient in nature (Fig. 4D,E).

Stereochemical basis of the specificity of IDOL for UBE2Ds

To understand why IDOL requires UBE2Ds and does not degrade the LDLR in combination with other E2 ligases, we carefully examined residues at the interface of the complex. It appears that residues in two positions in the interface play an important role in determining specificity. Arg15 is conserved in UBE2D1–4. Together with Lys8, Arg15 provides a basic pocket that accommodates the acidic side chain of Glu383 in the IDOL RING (Fig. 5A). In nearly all of the E2s that do not support IDOL-mediated degradation of the LDLR, the residue at this position is

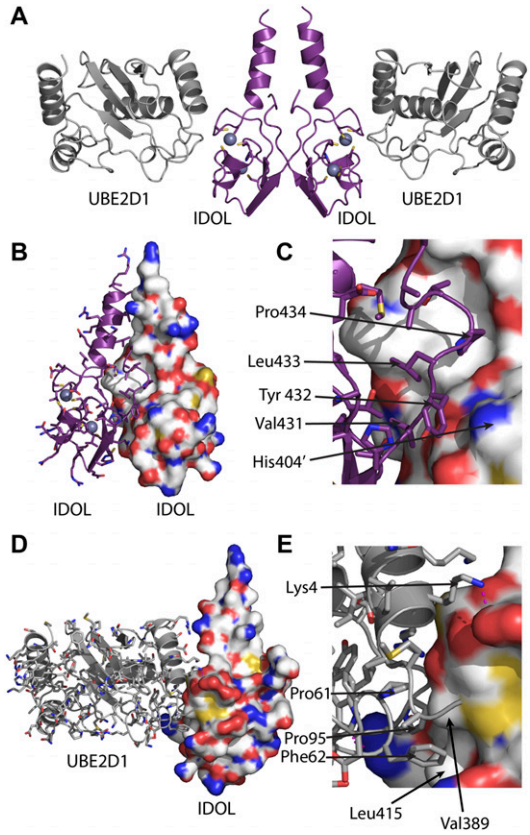

Figure 4. Crystal structure of the IDOL RING domain dimer complexed with UBE2D1. (*A*) Cartoon representation with the IDOL RING is shown in purple, and the UBE2D1 is shown in gray. (*B*) The RING domain dimer interface. (*C*) Close-up of the RING domain dimer interface. (*D*) The interface of the IDOL RING domain with UBE2D1. (*E*) Close-up of the IDOL RING–UBE2D1 complex interface.

either uncharged or acidic. Due to the close proximity of Asp16, either a neutral or acidic residue at position 15 results in an acidic surface that would perturb interaction of the E2 with the IDOL RING domain, as is the case for UBE2E3 (see inset in Fig. 5A). All of the E2 ligases that do have an arginine or lysine equivalent to Arg15 in UBE2Ds are lacking a key serine residue (Ser94 in UBE2D1) at the other end of the interface (Fig. 5B,C). This serine side chain makes a critical hydrogen bond to the backbone carbonyl oxygen of Pro419 in IDOL, and this in turn brings about a tight stacking of the rings of Pro95 in UBE2D1 and Pro419 in IDOL. In UBE2L3, UBE2G1, and UBE2T, the serine is substituted by much larger side chains (Lys, Leu, and Arg, respectively), which could not be accommodated at the interface with IDOL.

Disruption of the IDOL RING domain–UBE2D interaction inhibits LDLR degradation

Based on our structural data, we generated targeted mutations to further interrogate the IDOL–UBED2 interaction. The structure suggested that Val389 and Leu415 were potentially critical IDOL residues mediating hydrophobic interactions with UBE2D1 (Fig. 4E). In order to validate these predictions, we expressed LDLR together with native or tagged IDOL mutants in HEK293 cells. Compared with wild-type IDOL, the IDOL mutants V389R and L415E exhibited reduced capacity for LDLR degradation (Fig. 6A). Interestingly, the autodegradation of IDOL was also clearly inhibited by the introduction of the V389R and L415E mutations. We also performed an in vitro auto-ubiquitination assay using IDOL V389R. Consistent with the cellular results, UBE2D2 was unable to efficiently catalyze the polyubiquitination of the IDOL V389R mutant (Fig. 6B). Furthermore, introduction of mutations in Pro61 and Phe62 in UBE2D2 (P61A and F62R), residues that are buried at the hydrophobic E2–E3 interface, also inhibited the ability of UBE2D2 to support IDOL autoubiquitination (Fig. 6C).

Mutational analyses also validated our model for IDOL–UBE2D specificity outlined in Figure 5. Residue Glu383 in IDOL interacts with a basic pocket formed by Arg15 and Lys8 of UBE2D. Mutation of these basic residues in UBE2D2 (R15E and K8E) reduced the ability of UBE2D2 to support IDOL autoubiquitination in vitro (Fig. 6D). Our model further predicts that Ser94 of UBE2D, which makes an important hydrogen bond with the IDOL backbone, is a key determinant of specificity. UBE2L3, which is unable to pair with IDOL, has a lysine residue in this position (Fig. 5B,C). In support of our model, a UBE2D2 S94K mutant

Table 1. *Data collection and refinement statistics*

	IDOL (369–445)	IDOL (369–445) UBE2D1
Data collection		
Space group	I 1 2 1	P 1 21 1
Cell dimensions		
a, *b*, *c* (Å)	79.26, 22.77, 87.84	57.69, 137.87, 63.75
α, β, γ (°)	90.00, 116.82, 90.00	90.00, 106.39, 90.00
Resolution (Å)	39.19–3.00 (3.16–3.00)	55.91–2.10 (2.21–2.1)
R_{sym} or R_{merge}	13.8 (34.4)	8.9 (35.5)
$I/\sigma I$	12.2 (7.4)	9.0 (3.2)
Completeness (%)	99.2 (100.0)	99.6 (99.8)
Redundancy	3.9 (4.0)	3.5 (3.6)
Refinement		
Resolution (Å)	3.00	2.1
Number of reflections	2928	53,163
R_{work}/R_{free}	22.84 (29.7)	18.56 (23.33)
Number of atoms		
Protein	880	6766
Water		406
Acetate		36
B-factors		
Protein and acetate	21.88	31.26
Water		33.30
RMSDs		
Bond lengths (Å)	0.019	0.008
Bond angles (°)	0.842	1.158

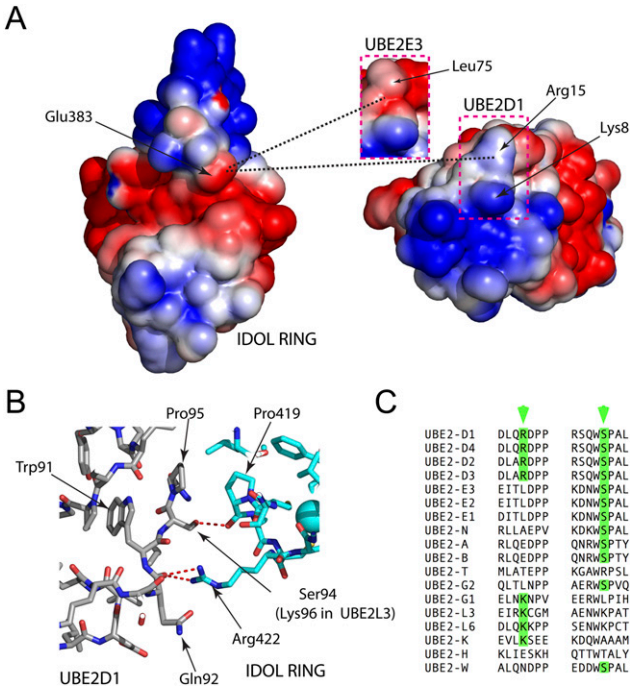

Figure 5. Specificity determinants for the IDOL RING:UBE2D interaction. (*A*) Electrostatic potential of the interface between the IDOL RING domain (*left*) and UBE2D1 (*right*). Note that the main interaction surface on the E2 is highly basic, and the complementary surface on the E3 is acidic. Arg15 in UBE2D1 provides a basic pocket to accommodate Glu383 from IDOL. (*Insert*) In noncomplementary E2s such as UBE2E3, the residue in this position is neutral or acidic and disfavors interaction. (*B*) Some E2s that are noncomplementary with IDOL have a basic residue in position 15, but an important serine at the interface (Ser94 in UBE2D1) is substituted with other amino acids, such as lysine in UBE2L3. The serine makes an important backbone contact that could not be formed by the alternative residues. (*C*) Alignment of key regions of various E2 ligases. Only members of the UBE2D family have both a basic residue and a serine to support appropriate interactions with the IDOL RING.

exhibited markedly reduced ability to catalyze IDOL autoubiquitination.

As the crystal structure of the IDOL RING domain–UBE2D complex revealed that IDOL could form a dimer via the residues within the RING domain, we performed coimmunoprecipitation experiments to validate the physiological relevance of this finding. We found that, when coexpressed with a V5-tagged IDOL in HEK293 cells, TAP-IDOL could be coimmunoprecipitated with the V5-tagged IDOL (Fig. 6E). These data indicated that the two different tagged versions of IDOL could form a complex in the cell. Furthermore, introduction of structure-guided mutations predicted to disrupt dimer formation (V431R/L433R) abolished the ability of TAP-IDOL and V5-IDOL to be coimmunoprecipitated from cells (Fig. 6F). Moreover, IDOL dimer formation appears to be essential for its biological function, because the dimer-defective mutant V431R/L433R was unable to promote LDLR degradation and was resistant to autocatalyzed degradation (Fig. 6G).

Based on these results, we reasoned that overexpression of IDOL mutants not capable of interacting with their cognate E2s should interact with and sequester wild-type IDOL molecules, thereby preventing them from participating in ubiquitin transfer. Such mutant IDOL proteins should therefore function as dominant negatives. To test this hypothesis, we coexpressed increasing amounts of IDOL V389R with a predetermined amount of wild-type IDOL and LDLR in HEK293 cells. Indeed, expression of IDOL V389R inhibited the degradation of LDLR by the wild-type IDOL in a dose-dependent manner (Fig. 6H). Furthermore, the autodegradation of wild-type IDOL was also inhibited by expression of the V389R mutant.

IDOL is an iron-binding protein

Immediately N-terminal to the crystallized IDOL RING construct, there are three cysteine residues (Cys360, Cys363, and Cys368) (Fig. 7A,B). Expression and purification of an extended RING domain containing residues 358–445 yield a brown protein (Fig. 7C–E). Other constructs of IDOL containing this region, including the full-length protein, are also brown (data not shown). Atomic absorption spectroscopy was performed on both IDOL RING constructs to measure the metal content in comparison with zinc and iron standards. For the shorter 369–445 construct, a 0.24 mM protein sample gave a zinc concentration of 0.47 mM and an iron concentration of 0.012 mM; for the longer 358–445 construct, a 0.15 mM protein sample gave a zinc concentration of 0.3 mM and an iron concentration of 0.06 mM (Fig. 7C). These concentrations correspond to two zinc ions per protein molecule and one iron ion per dimer for the longer protein. Protein disorder prediction of IDOL using RONN (Yang et al. 2005) suggests that most of IDOL is ordered, but that amino acids 332–371 are inherently disordered. It is therefore possible that this region contributes to the dimerization interface when folded around an iron ion.

In order to address the potential functional significance of this iron-binding region, we introduced mutations into each of the three cysteine residues, alone or in combination (Fig. 7F). Unexpectedly, these mutations led to increased LDLR degradation activity compared with wild-type IDOL. Analysis of TAP-IDOL expression revealed that the increased LDLR degradation in these experiments likely resulted from increased IDOL stability. Levels of IDOL protein expression were increased in an additive manner with mutation of C360, C363, and C368 (Fig. 7F), with the most prominent effects observed with the triple mutant (IDOL AAA) (Fig. 7G). The data suggest that the structure of the IDOL protein in the presence of iron may be more conducive to autoubiquitination and degradation.

Finally, LDL uptake studies confirmed the functional consequences of the dimerization, E2 interaction, and iron-binding mutations. The E2 interaction mutants (V389R and L415E) and the dimerization mutant (L433R/V431R) reduced IDOL activity, whereas the iron-binding mutant (IDOL AAA) actually increased IDOL's ability to block LDL uptake (Fig. 7H). Thus, our combination of biochemical and structural analyses has

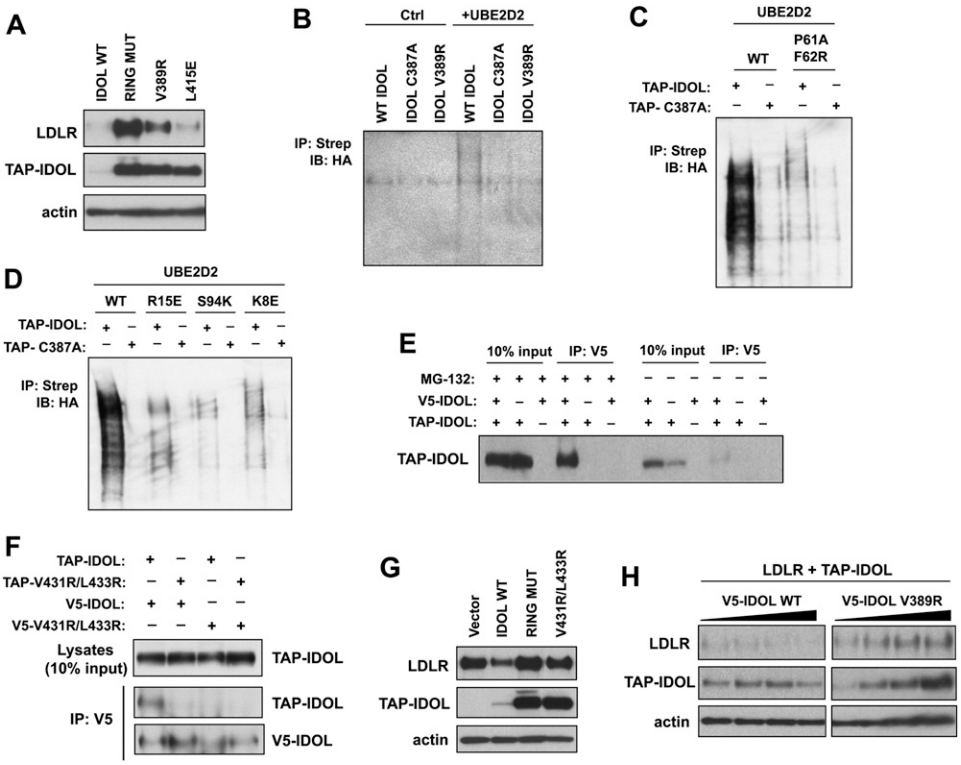

Figure 6. Disruption of the IDOL–UBE2D interaction blocks LDLR degradation. (*A*) Mutations in the IDOL RING domain–UBE2D interaction interface inhibit LDLR degradation. Immunoblot analysis of protein levels in 293 cells transfected with LDLR and wild-type (WT) or mutant IDOL expression vectors. (*B*) UBE2D is unable to catalyze the autoubiquitination of mutant IDOL with a disrupted IDOL RING domain–UBE2D interaction. Immunoprecipitated TAP-IDOL, TAP-IDOL C387A, and TAP-IDOL V389R were incubated with UBE1, UBE2D2, and HA-ubiquitin. IDOL ubiquitination was detected by Western blot for HA-tagged ubiquitin associated with IDOL. (*C*) UBE2D2 mutated at the interface with IDOL is unable to catalyze IDOL autoubiquitination. Immunoprecipitated TAP-IDOL and TAP-IDOL C387A were incubated with UBE1, wild-type, or P61A/F62R UBE2D2 and HA-ubiquitin. IDOL ubiquitination was detected by Western blot for HA-tagged ubiquitin associated with IDOL. (*D*) Mutation of UBE2D2 residues predicted to be involved in IDOL specificity determination reduces the ability of UBE2D2 to support IDOL autoubiquitination. Immunoprecipitated TAP-IDOL and TAP-IDOL C387A were incubated with UBE1, wild-type, R15E, S94K, or K8E UBE2D2 and HA-ubiquitin. IDOL ubiquitination was detected by Western blot for HA-tagged ubiquitin associated with IDOL. (*E*) IDOL forms a dimer in vivo. 293 cells were transfected with vectors expressing TAP-IDOL and V5-IDOL. V5-IDOL in the cell lysate was immunoprecipitated with an anti-V5 antibody. The TAP-IDOL that coimmunoprecipitated with V5-IDOL was detected by immunoblotting using an anti-Flag antibody. (*F*) Structure-based mutations predicted to disrupt dimer formation prevent the coimmunoprecipitation of TAP-IDOL and V5-IDOL. 293 cells were transfected with the indicated combination of expression vectors. V5-IDOL and V5-mutant IDOL in the cell lysate were immunoprecipitated with an anti-V5 antibody. The coimmunoprecipitated TAP-IDOL was detected by immunoblotting using anti-Flag. (*G*) A dimer-defective IDOL mutant is unable to induce LDLR degradation. Immunoblot analysis of protein levels in 293 cells transfected with LDLR and wild-type or mutant IDOL expression vectors. (*H*) IDOL harboring a mutation in the IDOL RING domain–UBE2D interaction interface functions as a dominant negative in LDLR degradation assays. Immunoblot analysis of protein levels in 293 cells transfected with increasing amounts of V5-tagged wild-type or mutant IDOL, in addition to constant levels of LDLR and TAP-IDOL.

defined molecular interactions critical for the LXR–IDOL–LDLR sterol regulatory pathway.

Discussion

In this study, we identified the ubiquitin-conjugating enzyme E2D family proteins (UBE2D1–4) as the E2 ubiquitin carrier proteins involved in IDOL-dependent LDLR ubiquitination. Our results provide strong evidence that IDOL directly facilitates the transfer of ubiquitin to LDLR by acting in a complex with UBE2D. We also successfully carried out a biochemical and structural characterization of the E2–E3 complex, and demonstrated that disruption of UBE2D activity or the interaction interface between UBE2D and IDOL inhibits the degradation of the LDLR. These results provide a better understanding of the molecular mechanism underlying the sterol-dependent regulation of LDLR protein levels.

Since the LDLR is a membrane protein, it is challenging to study IDOL–LDLR interaction in a cell-free system. Our available assays for IDOL-dependent LDLR ubiquitination were not amenable to the screening of potential E2 enzymes. We therefore used an alternative approach that assayed the autoubiquitination of IDOL in

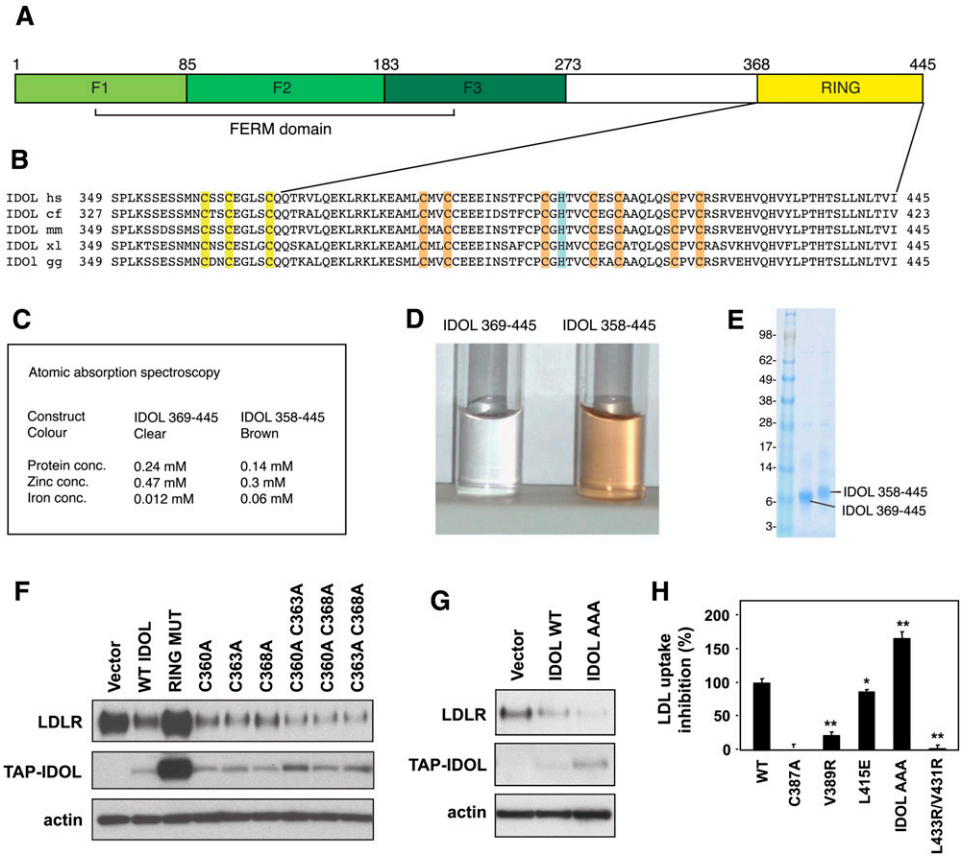

Figure 7. IDOL is an iron-binding protein. (*A*) Schematic diagram of the domain structure of IDOL. (*B*) Alignment of IDOL sequences: (hs) *Homo sapiens*; (cf) *Canis familiaris*; (mm) *Mus musculus*; (xl) *Xenopus laevis*; (gg) *Gallus gallus*. The three conserved Cys residues N-terminal to the RING domain are highlighted in yellow. The Cys zinc ligands are highlighted in orange, and the His zinc ligand is highlighted in blue. (*C*) Results from atomic absorption spectroscopy. (*D*) Photograph of protein samples of IDOL constructs eluted from glutathione Sepharose by cleavage with TEV protease. (*E*) Coomassie-stained SDS-PAGE gel of IDOL constructs eluted from glutathione Sepharose by cleavage with TEV protease. (*F,G*) Disruption of the putative iron-binding cysteine residues alters IDOL stability and LDLR degradation. Immunoblot analysis of protein levels in 293 cells transfected with LDLR and wild-type (WT) or mutant IDOL expression vectors. (*H*) Effect of IDOL interaction mutants on the ability of IDOL to inhibit LDL uptake. 293 cells were transfected with LDLR and wild-type or mutant IDOL expression vectors and then incubated for 4 h with DiI-labeled LDL. Cells were washed and associated cellular LDL were quantified by fluorescence. Results are presented as percent wild-type (% WT) IDOL inhibitory activity in LDL uptake assays. The inhibitory activity of wild-type IDOL was defined as 100%, and that of the inactive RING mutant (C387A) was defined as 0. (**) $P < 0.001$; (*) $P < 0.05$.

vitro. Autoubiquitination is characteristic of RING-type E3 ligases. It is achieved via the same chemical reaction as the ubiquitin-substrate ligation and is mediated by the same E2 protein (Yang et al. 2000). We screened 19 candidate E2 enzymes identified previously as preferentially interacting with the RING-type E3 ligases (Markson et al. 2009; van Wijk et al. 2009). Of these, proteins in the UBE2D family were the only ones that were able to catalyze IDOL autoubiquitination in vitro. Although unlikely, it remains possible that additional E2 enzymes not predicted to interact with RING E3, and therefore omitted from our analysis, could also interact with IDOL. Therefore, we cannot formally exclude the existence of additional E2 proteins capable of mediating IDOL-dependent ubiquitination.

Although we initially identified the IDOL–UBE2D interaction based on IDOL autoubiquitination, several lines of evidence indicate that the UBE2D family enzymes also mediate the ubiquitination and degradation of the LDLR. We showed that UBE2D2, together with recombinant E1 and purified IDOL, was able to induce ubiquitination of LDLR in cell-free membrane preparations in vitro. In addition, we demonstrated that the inhibition of UBE2D activity by overexpressing a dominant-negative UBE2D enzyme inhibited the ability of IDOL to degrade the LDLR in cells. These dominant-negative enzymes are postulated to function by interacting with the E3 enzyme and consequently prevent it from associating with endogenous E2 (Gonen et al. 1999).

We also successfully obtained the crystal structure of the IDOL RING domain–UBE2D complex. The E2 ubiquitin-conjugating enzymes are structurally related, and they share a conserved core domain with ~150 amino acids harboring the cysteine residues required for the formation

of the ubiquitin-E2 thioester intermediate (Zheng et al. 2000). Binding of an E2 to a RING-type E3 is dependent on the E3 RING finger domain, which contains one histidine and seven cysteine residues that coordinate with two zinc ions (Joazeiro and Weissman 2000). The RING-based E3s share many structural similarities in their RING domains, as do different E2s in their E2 core domains. Consequently, the biophysical basis for the specific functional pairings between E2s and E3s in E3 autoubiquitination as well as the ubiquitination of substrates has been a long-standing puzzle. Careful examination of the structure of the complex and comparison of the sequences of the E2s that do and do not support IDOL activity have enabled us to identify residues at two key positions at the interface that appear to determine specificity. Structure-guided mutations in UBE2D further supported this model. Our observations fit with early studies that suggested that the specificity of E2:E3 pairings is determined by the specific and complementary chemistry of the different intermolecular interfaces (Dominguez et al. 2004).

However, it is important to note that specificity may not be dependent on only the stereochemistry of the interface, but may also require optimal dynamics of association/dissociation. This is important because it is well-established that the E1- and E3-binding surfaces on the E2 are overlapping and that binding is mutually exclusive. This fits well with the observation that the interface between the IDOL RING and UBE2D1 is relatively small (1140 $Å^2$), which is consistent with the reported dissociation constants of interaction of RING domains with E2s typically >100 μM (Ozkan et al. 2005; Das et al. 2009). Thus, the dynamics of E2:E3 and E2:E1 interactions play a role in controlling ubiquitination of the target protein (van Wijk and Timmers 2010). Too tight an E2:E3 complex would block the E2:E1 interaction, and vice versa.

The finding that IDOL is an iron-binding protein raises the obvious question as to whether the iron is regulating the activity of the protein. We do not yet have any answers to this question, but it is provocative to note that iron has been implicated in heart disease (Sullivan 1996) and that studies of iron depletion show a lowering of LDL cholesterol (Facchini and Saylor 2002).

Based on the information provided by the crystal structure of the UBE2D–IDOL complex, we found that disruption of the interaction interface between IDOL and UBE2D not only inhibited the autoubiquitination of IDOL in an in vitro assay, but also prevented functional ubiquitination and degradation of the LDLR mediated by IDOL in cells. It has been generally assumed that the binding between an E2 and an E3 is the primary determinant of a functional E2–E3 pair. However, it has been shown that, although c-Cbl and UbcH7 form a complex, UbcH5B, rather than UbcH7, appears to be the functional E2 for the c-Cbl-mediated ubiquitination (Huang et al. 2009). It has also been reported that the BRCA1/BARD1 E3 heterodimer can interact with UbcH5C and UbcH7 with similar affinity, but only UbcH5C is active in ubiquitination assays (Brzovic et al. 2003). Results from these studies suggest that the physical binding between E2–E3 pairs is not sufficient to infer biological function, highlighting the importance of complementary structural and functional assays of E2–E3 interactions.

In summary, we identified and characterized an E2–E3 complex involved in the ubiquitination and degradation of the LDLR. This study furthers our understanding of the molecular mechanism underlying the regulation of the abundance of the LDLR by the ubiquitination system, and also provides a basis for future investigation of the functions of UBE2D and IDOL in the control of cholesterol metabolism.

Materials and methods

Plasmids and constructs

The pSA2-N-TAP plasmid that contains the 3xFlag-Strep tag and the pcDNA-V5-Dest plasmid were kindly provided by Dr. Enrique Saez (The Scripps Research Institute). The pDONR221 and pET300N-Dest plasmids were purchased from Invitrogen. The DNA sequence of the human Idol gene was amplified from a pcDNA-V5::hIdol construct as reported previously (Zelcer et al. 2009), and was then subcloned into a pSA2-N-TAP plasmid. The IDOL mutations for the pcDNA-V5::hIdol and pSA2-N-TAP::hIdol constructs were introduced by site-directed mutagenesis. The human E2 genes were cloned from HEK293 cell cDNA and were then sequentially subcloned into pDONR221 and pET300N-Dest using the Gateway technology (Invitrogen). In addition, the human Ube2d2 and Ube2h genes in the pDONR221::hUbe2d2 and pDONR221::hUbe2h constructs were subcloned into a pcDNA-V5-Dest plasmid using the Gateway technology. All mutations were introduced by site-directed mutagenesis.

Antibodies

Rabbit anti-hLDLR antibody was purchased from Cayman Chemicals. Rabbit anti-actin and mouse anti-Flag M2 antibodies were purchased from Sigma. Mouse anti-V5 antibody, HRP-conjugated goat anti-mouse IgG, and goat anti-rabbit IgG were purchased from Invitrogen. Rabbit anti-V5 antibody was purchased from Abcam. Rabbit anti-GFP antibody was purchased from Clontech. Mouse anti-HA antibody was purchased from Covance. All commercially available antibodies were used according to the manufacturers' instructions.

Cell culture and transfection

HEK293 cells were maintained in DMEM (Invitrogen) supplemented with 10% fetal bovine serum (Omega), 2 mM L-glutamine (Invitrogen), 50 U/mL penicillin (Invitrogen), and 50 μg/mL streptomycin (Invitrogen). Cells were grown in a humidified incubator at 37°C and 5% CO_2 atmosphere. HEK293 cells were transfected using FuGENE 6 reagents (Roche) according to the manufacturer's instructions. Clonal stable cell lines expressing IDOL were established by serial dilution selection with 2 μg/mL puromycin (Clontech).

Immunoblotting

Proteins were resolved on a 4%–12% gradient SDS-PAGE (Invitrogen) using standard protocols. The protein was electrophoretically transferred to nitrocellulose membranes (Amersham Biosciences) and blocked with milk solution (150 mM NaCl, 20 mM Tris, 5% milk, 0.2% Tween at pH 7.5) to quench nonspecific protein binding.

The blocked membranes were probed sequentially with primary and secondary antibodies diluted in the milk solution, and the bands were visualized with the ECL kit (Amersham Biosciences).

IDOL autoubiquitination assay

To prepare the *E. coli* lysates containing human UBE2 proteins, the BL21(DE3) strain (New England Biolabs) of *E. coli* containing various pET300N::hUbe2 constructs was cultured in LB broth (Sigma) overnight at 37°C. The bacteria cultures were then diluted 1:10 in LB broth and cultured for another 1–2 h at 37°C until OD_{600} reached ~0.8, at which point a final concentration of 1 mM IPTG was added to induce the expression of the UBE2 proteins. Two hours after the addition of IPTG, bacteria were collected in Eppendorf tubes, washed with PBS, and then sonicated using a thin-tip sonicater (Misonix). Crude lysate was cleared by centrifugation at 12,000*g* for 10 min, and the supernatant was collected for the in vitro autoubiquitination assays.

3xFlag-Strep-tagged human IDOL, IDOL C387A, IDOL V389R, and EGFP were expressed in HEK293 cells. Cells were lysed in RIPA buffer (Boston BioProducts, Inc.) supplemented with the Complete protease inhibitor cocktail (Roche). Cell lysate was cleared by centrifugation at 12,000*g* for 10 min, and the supernatant was then incubated with Streptactin beads (IBA GmbH) for 2 h at 4°C. The beads were then extensively washed with RIPA buffer before the in vitro autoubiquitination assays.

For each in vitro autoubiquitination assay, 25 μL of IDOL- or EGFP-bound Streptactin beads were mixed with 5 μL of *E. coli* lysate containing UBE2, 50 ng of recombinant rabbit UBE1 (Calbiochem), and 10 μg of recombinant HA-ubiquitin (Boston Biochem). The reaction buffer contained 50 mM Tris-HCl (pH 7.4), 5 mM $MgCl_2$, 2 mM ATP, and 25 μM MG132 (Sigma). The reaction mixture was incubated for 1 h at 37°C. After the reaction, the Streptactin beads were separated and then extensively washed with RIPA buffer before the proteins on the beads were eluted by heated protein loading buffer (Invitrogen). Ubiquitination status was analyzed by immunoblotting using an anti-HA antibody.

LDLR ubiquitination assay

HEK293 cells expressing LDLR-GFP or GFP control were permeabilized, and the cytosolic proteins were removed according to a protocol published previously (Song and DeBose-Boyd 2004). IDOL and IDOL C387A stably expressed in HEK293 cells were purified using a tandem affinity purification protocol (Gloeckner et al. 2009). For each in vitro ubiquitination assay, 25 μL of pelleted permeabilized cells were mixed with 2 μL of purified IDOL, 2 μL of *E. coli* lysate containing UBE2, 50 ng of recombinant rabbit UBE1, and 10 μg of recombinant HA-ubiquitin. The reaction buffer contained 50 mM Tris-HCl (pH 7.4), 5 mM $MgCl_2$, 2 mM ATP, and 25 μM MG132 (Sigma). The reaction mixture was incubated for 1 h at 37°C. After the reaction, the permeabilized cells were separated and lysed in RIPA buffer supplemented with the Complete protease inhibitor cocktail. The cell lysate was then cleared by centrifugation at 12,000*g* for 10 min. LDLR in the lysate was immunoprecipitated with a rabbit anti-GFP antibody and protein G beads (Santa Cruz Biotechnology), and the ubiquitination status of LDLR was analyzed by immunoblotting using an anti-HA antibody.

NMR spectroscopy

For the NMR experiments, ^{15}N-^{13}C His-tagged IDOL 369–445 was purified on Ni-NTA (Qiagen) and, after TEV cleavage of the tag, was purified further on a Resource-Q column (GE Healthcare). The protein was transferred into 20 mM sodium phosphate, 150 mM NaCl, and 0.25 mM TCEP using a PD10 (GE Healthcare) and concentrated to 0.6 mM immediately prior to collection of NMR spectra. NMR experiments for the resonance assignment of IDOL 369–445 were carried out with 0.6 mM protein in 20 mM sodium phosphate (pH 6.5), 100 mM NaCl, and 10% (v/v) ^2H_2O. NMR spectra of all the proteins were obtained at 298 K using Bruker AVANCE DRX 600 or AVANCE DRX 800 spectrometers, both equipped with CryoProbes. Proton chemical shifts were referenced to external 2,2-dimethyl-2-silapentane-5-sulfonic acid, and ^{15}N and ^{13}C chemical shifts were referenced indirectly using recommended gyromagnetic ratios (Wishart et al. 1995). Spectra were processed with TopSpin (Bruker Corp.) and analyzed using Analysis (Vranken et al. 2005). Three-dimensional HNCO, HN(CA)CO, HNCA, HN(CO)CA, HNCACB, and HN(CO)CACB experiments were used for the sequential assignment of the backbone NH, N, CO, Cα, and Cβ resonances.

Crystallization and X-ray structure determination

For the crystallization experiments, GST-tagged IDOL 369–445 was purified using glutathione sepharose resin (GE Healthcare), eluted by TEV cleavage, and purified further on a Resource-Q (GE Healthcare). His-tagged UBE2D1 was purified on Ni-NTA (Qiagen) and, after TEV-cleavage of the tag, on a Superdex-75 column (GE Healthcare). IDOL 369–445 alone was concentrated to 7.5 mg/mL in a buffer containing 50 mM Tris (pH 8), 100 mM NaCl, and 0.5 mM TCEP. IDOL RING domain alone was crystallized from 0.1 M sodium acetate (pH 7–8) and 16%–20% MPD in the space group I 1 2 1. For the complex crystals, the two proteins were concentrated independently, mixed at equimolar concentrations, and crystallized from 0.1 M sodium citrate (pH 5.5), 0.2 M sodium acetate, and 10% PEG 4000 in the space group P 1 21 1. Data were collected at the synchrotron at ESRF on ID23-1 to 3.0 Å for the RING domain alone and at Diamond on I04 (to 2.1 Å) for the complex. The data were processed using MOSFLM (Leslie 2006), and both structures were solved by molecular replacement using Phaser (Mccoy et al. 2007). The model for the RING domain alone was taken from the cIAP RING structure (3EB5) (Mace et al. 2008). The complex was solved by using the 3 Å IDOL 369–445 domain structure and the UBE2D2 structure from 3EB6 (Mace et al. 2008). The UBE2D2 complexed with cIAP (3EB6) was not a successful search model, as the two proteins have moved with respect to each other in the IDOL 369–445 UBE2D1 structure. Model building and refinement were performed using Coot, REFMAC, and Phenix (Collaborative Computational Project, Number 4 1994; Adams et al. 2010; Emsley et al. 2010). The crystallographic statistics are shown in Table 1.

Atomic absorption spectroscopy

For the atomic absorption spectroscopy, GST-tagged IDOL 358–445 and GST-tagged IDOL 369–445 were purified as described above. Zinc and iron standards were used. The zinc concentration for the brown IDOL 358–445 was 0.3 mM, and the iron concentration was 0.06 mM. The zinc concentration for the clear IDOL 369–445 was 0.47 mM, and the iron concentration was 0.012 mM.

Accession numbers

Coordinates and structure factors for the IDOL RING domain and the IDOL RING domain–UBE2D1 complex crystal structures have been deposited in the Protein Data Bank (ID codes 2YHN and 2YHO, respectively), and the ^1H, ^{15}N, and ^{13}C NMR chemical shifts for the IDOL RING domain have been deposited in the BioMagResBank database (accession code 17550).

Acknowledgments

We thank Stephen Young and members of the Tontonoz and Schwabe laboratories for helpful discussions. We thank Andrea Gumiero and Jonas Elmsley for help with data collection, Arnoud Boom for the atomic absorption spectroscopy, Jennifer Kwan for some initial crystallization trials, and the PROTEX facility at Leicester for generating many of the expression constructs. J.W.R.S., B.T.G., L.F., and P.T. are supported by Wellcome Trust grants WT091820 and WT085408. P.T. is an investigator of the Howard Hughes Medical Institute and was also supported by NIH grants HL090553 and HL030568. A.C.C. is funded by a National Heart Foundation of Australia Overseas Fellowship (O 08M 3934).

References

Adams PD, Afonine PV, Bunkoczi G, Chen VB, Davis IW, Echols N, Headd JJ, Hung LW, Kapral GJ, Grosse-Kunstleve RW, et al 2010. PHENIX: a comprehensive Python-based system for macromolecular structure solution. *Acta Crystallogr D Biol Crystallogr* **66:** 213–221.

Barlow PN, Luisi B, Milner A, Elliott M, Everett R. 1994. Structure of the C3HC4 domain by ^{1}H-nuclear magnetic resonance spectroscopy. A new structural class of zinc-finger. *J Mol Biol* **237:** 201–211.

Brown MS, Goldstein JL. 1986. A receptor-mediated pathway for cholesterol homeostasis. *Science* **232:** 34–47.

Bruford EA, Lush MJ, Wright MW, Sneddon TP, Povey S, Birney E. 2008. The HGNC Database in 2008: a resource for the human genome. *Nucleic Acids Res* **36:** D445–D448. doi: 10.1093/nar/gkm881.

Brzovic PS, Keeffe JR, Nishikawa H, Miyamoto K, Fox D III, Fukuda M, Ohta T, Klevit R. 2003. Binding and recognition in the assembly of an active BRCA1/BARD1 ubiquitin-ligase complex. *Proc Natl Acad Sci* **100:** 5646–5651.

Collaborative Computational Project, Number 4. 1994. The CCP4 suite: programs for protein crystallography. *Acta Crystallogr D Biol Crystallogr* **50:** 760–763.

Das R, Mariano J, Tsai YC, Kalathur RC, Kostova Z, Li J, Tarasov SG, McFeeters RL, Altieri AS, Ji X, et al 2009. Allosteric activation of E2-RING finger-mediated ubiquitylation by a structurally defined specific E2-binding region of gp78. *Mol Cell* **34:** 674–685.

Deshaies RJ. 1999. SCF and Cullin/Ring H2-based ubiquitin ligases. *Annu Rev Cell Dev Biol* **15:** 435–467.

Dominguez C, Bonvin AM, Winkler GS, van Schaik FM, Timmers HT, Boelens R. 2004. Structural model of the UbcH5B/CNOT4 complex revealed by combining NMR, mutagenesis, and docking approaches. *Structure* **12:** 633–644.

Dye BT, Schulman BA. 2007. Structural mechanisms underlying posttranslational modification by ubiquitin-like proteins. *Annu Rev Biophys Biomol Struct* **36:** 131–150.

Emsley P, Lohkamp B, Scott WG, Cowtan K. 2010. Features and development of Coot. *Acta Crystallogr D Biol Crystallogr* **66:** 486–501.

Facchini FS, Saylor KL. 2002. Effect of iron depletion on cardiovascular risk factors: studies in carbohydrate-intolerant patients. *Ann NY Acad Sci* **967:** 342–351.

Gloeckner CJ, Boldt K, Schumacher A, Ueffing M. 2009. Tandem affinity purification of protein complexes from mammalian cells by the Strep/Flag (SF)-TAP tag. *Methods Mol Biol* **564:** 359–372.

Goldstein JL, DeBose-Boyd RA, Brown MS. 2006. Protein sensors for membrane sterols. *Cell* **124:** 35–46.

Gonen H, Bercovich B, Orian A, Carrano A, Takizawa C, Yamanaka K, Pagano M, Iwai K, Ciechanover A. 1999. Identification of the ubiquitin carrier proteins, E2s, involved in signal-induced conjugation and subsequent degradation of IκBα. *J Biol Chem* **274:** 14823–14830.

Hershko A, Ciechanover A. 1998. The ubiquitin system. *Annu Rev Biochem* **67:** 425–479.

Hua X, Yokoyama C, Wu J, Briggs MR, Brown MS, Goldstein JL, Wang X. 1993. SREBP-2, a second basic-helix–loop–helix–leucine zipper protein that stimulates transcription by binding to a sterol regulatory element. *Proc Natl Acad Sci* **90:** 11603–11607.

Huang A, de Jong RN, Wienk H, Winkler GS, Timmers HT, Boelens R. 2009. E2-c-Cbl recognition is necessary but not sufficient for ubiquitination activity. *J Mol Biol* **385:** 507–519.

Joazeiro CA, Weissman AM. 2000. RING finger proteins: mediators of ubiquitin ligase activity. *Cell* **102:** 549–552.

Koepp DM, Harper JW, Elledge SJ. 1999. How the cyclin became a cyclin: regulated proteolysis in the cell cycle. *Cell* **97:** 431–434.

Leslie AG. 2006. The integration of macromolecular diffraction data. *Acta Crystallogr D Biol Crystallogr* **62:** 48–57.

Levkowitz G, Waterman H, Ettenberg SA, Katz M, Tsygankov AY, Alroy I, Lavi S, Iwai K, Reiss Y, Ciechanover A, et al. 1999. Ubiquitin ligase activity and tyrosine phosphorylation underlie suppression of growth factor signaling by c-Cbl/Sli-1. *Mol Cell* **4:** 1029–1040.

Mace PD, Linke K, Feltham R, Schumacher FR, Smith CA, Vaux DL, Silke J, Day CL. 2008. Structures of the cIAP2 RING domain reveal conformational changes associated with ubiquitin-conjugating enzyme (E2) recruitment. *J Biol Chem* **283:** 31633–31640.

Markson G, Kiel C, Hyde R, Brown S, Charalabous P, Bremm A, Semple J, Woodsmith J, Duley S, Salehi-Ashtiani K, et al. 2009. Analysis of the human E2 ubiquitin conjugating enzyme protein interaction network. *Genome Res* **19:** 1905–1911.

Maxwell KN, Breslow JL. 2004. Adenoviral-mediated expression of Pcsk9 in mice results in a low-density lipoprotein receptor knockout phenotype. *Proc Natl Acad Sci* **101:** 7100–7105.

Mccoy AJ, Grosse-Kunstleve RW, Adams PD, Winn MD, Storoni LC, Read RJ. 2007. Phaser crystallographic software. *J Appl Crystallogr* **40:** 658–674.

Ozkan E, Yu H, Deisenhofer J. 2005. Mechanistic insight into the allosteric activation of a ubiquitin-conjugating enzyme by RING-type ubiquitin ligases. *Proc Natl Acad Sci* **102:** 18890–18895.

Park SW, Moon YA, Horton JD. 2004. Post-transcriptional regulation of low density lipoprotein receptor protein by proprotein convertase subtilisin/kexin type 9a in mouse liver. *J Biol Chem* **279:** 50630–50638.

Pickart CM. 2001. Mechanisms underlying ubiquitination. *Annu Rev Biochem* **70:** 503–533.

Russell DW, Schneider WJ, Yamamoto T, Luskey KL, Brown MS, Goldstein JL. 1984. Domain map of the LDL receptor: sequence homology with the epidermal growth factor precursor. *Cell* **37:** 577–585.

Scheffner M, Werness BA, Huibregtse JM, Levine AJ, Howley PM. 1990. The E6 oncoprotein encoded by human papillomavirus types 16 and 18 promotes the degradation of p53. *Cell* **63:** 1129–1136.

Scheffner M, Huibregtse JM, Vierstra RD, Howley PM. 1993. The HPV-16 E6 and E6-AP complex functions as a ubiquitin-protein ligase in the ubiquitination of p53. *Cell* **75:** 495–505.

Song BL, DeBose-Boyd RA. 2004. Ubiquitination of 3-hydroxy-3-methylglutaryl-CoA reductase in permeabilized cells mediated by cytosolic E1 and a putative membrane-bound ubiquitin ligase. *J Biol Chem* **279:** 28798–28806.

Sullivan JL. 1996. Iron versus cholesterol–perspectives on the iron and heart disease debate. *J Clin Epidemiol* **49:** 1345–1352.

Thrower JS, Hoffman L, Rechsteiner M, Pickart CM. 2000. Recognition of the polyubiquitin proteolytic signal. *EMBO J* **19:** 94–102.

van Wijk SJ, Timmers HT. 2010. The family of ubiquitin-conjugating enzymes (E2s): deciding between life and death of proteins. *FASEB J* **24:** 981–993.

van Wijk SJ, de Vries SJ, Kemmeren P, Huang A, Boelens R, Bonvin AM, Timmers HT. 2009. A comprehensive framework of E2–RING E3 interactions of the human ubiquitin-proteasome system. *Mol Syst Biol* **5:** 295. doi: 10.1038/msb.2009.55.

Vranken WF, Boucher W, Stevens TJ, Fogh RH, Pajon A, Llinas M, Ulrich EL, Markley JL, Ionides J, Laue ED. 2005. The CCPN data model for NMR spectroscopy: development of a software pipeline. *Proteins* **59:** 687–696.

Wishart DS, Bigam CG, Yao J, Abildgaard F, Dyson HJ, Oldfield E, Markley JL, Sykes BD. 1995. ^{1}H, ^{13}C and ^{15}N chemical shift referencing in biomolecular NMR. *J Biol NMR* **6:** 135–140.

Yang Y, Fang S, Jensen JP, Weissman AM, Ashwell JD. 2000. Ubiquitin protein ligase activity of IAPs and their degradation in proteasomes in response to apoptotic stimuli. *Science* **288:** 874–877.

Yang ZR, Thomson R, McNeil P, Esnouf RM. 2005. RONN: the bio-basis function neural network technique applied to the detection of natively disordered regions in proteins. *Bioinformatics* **21:** 3369–3376.

Zelcer N, Hong C, Boyadjian R, Tontonoz P. 2009. LXR regulates cholesterol uptake through Idol-dependent ubiquitination of the LDL receptor. *Science* **325:** 100–104.

Zheng N, Wang P, Jeffrey PD, Pavletich NP. 2000. Structure of a c-Cbl–UbcH7 complex: RING domain function in ubiquitin-protein ligases. *Cell* **102:** 533–539.